Lightweight rovers for Mars science exploration and sample return

P. S. Schenker, L. F. Sword, A. J. Ganino, D. B. Bickler, G. S. Hickey, D. K. Brown,
E. T. Baumgartner, L. H. Matthies, B. H. Wilcox, T. Balch, H. Aghazarian and M. S. Garrett

Jet Propulsion Laboratory, California Institute of Technology
4800 Oak Grove Drive/MS 125-224
Pasadena, California 91109-8099
paul.s.schenker@jpl.nasa.gov

ABSTRACT

We report on the development of new mobile robots for Mars exploration missions. These "lightweight survivable rover (LSR)" systems are of potential interest to both space and terrestrial applications, and are distinguished from more conventional designs by their use of new composite materials, collapsible running gear, integrated thermal-structural chassis, and other mechanical features enabling improved mobility and environmental robustness at reduced mass, volume, and power. Our first demonstrated such rover architecture, ***LSR-1***, introduces running gear based on 2D composite struts and 3D machined composite joints, a novel collapsible hybrid composite-aluminum wheel design, a unit-body structural-thermal chassis with improved internal temperature isolation and stabilization, and a spot-pushbroom laser/CCD sensor enabling accurate, fast hazard detection and terrain mapping. LSR-1 is a ~ .7 x 1.0 meter^2(WxL) footprint six-wheel (20 cm dia.) rocker-bogie geometry vehicle of ~ 30 cm ground clearance, weighing only 7 kilograms with an onboard .3 kilogram multi-spectral imager and spectroscopic photometer. By comparison, NASA/JPL's recently flown Mars Pathfinder rover Sojourner is an 11+ kilogram flight experiment (carrying a 1 kg APXS instrument) having ~.45 x .6 meter^2 (WxL) footprint and 15 cm ground clearance, and about half the warm electronics enclosure (WEE) volume with twice the diurnal temperature swing (-40 to +40°C) of LSR-1 in nominal Mars environments. We are also developing a new, smaller 5 kilogram class LSR-type vehicle for Mars sample return – the travel to, localization of, pick-up, and transport back to an Earth return ascent vehicle of a sample cache collected by earlier science missions. This *Sample Retrieval Rover* R&D prototype has a completely collapsible mobility system enabling rover stowage to ~25% operational volume, as well an actively articulated axle, allowing changeable pose of the wheel strut geometry for improved traverse and manipulation characteristics.

Keywords: mobile robots, 3D sensing, robotic sampling, planetary science, Mars sample return

1. INTRODUCTION

As demonstrated by this year's NASA Mars Pathfinder (MPF) mission to Ares Valles, small rovers [1] will be important assets for future science exploration of planetary surfaces. Such vehicles will enable wide-area imaging and identification of science sites, spectroscopically-based chemical analysis of surface terrain and outcroppings, collection of loose soil and extracted rock samples, local meteorology and many other functions. This science data collection is fundamental to understanding the formative processes of Martian geology, mineralogy, climate; a possible history of life; and, suitability of the Martian environment to future habitation.

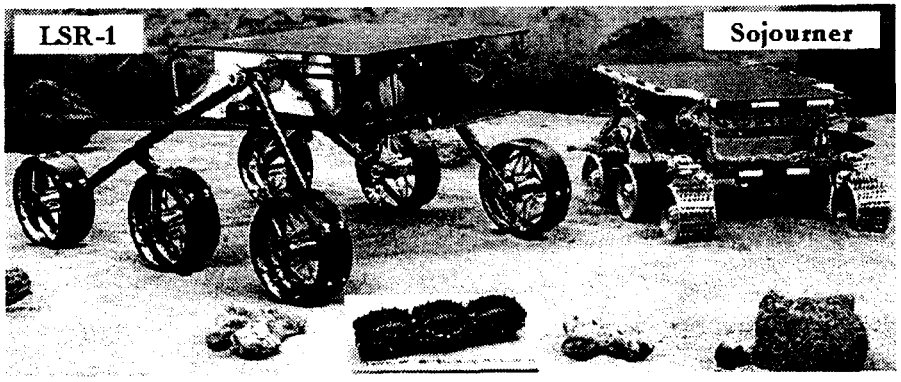

Figure 1. Lightweight Survivable Rover is shown at left, a 7 kg vehicle having about 4X the operational volume of NASA's Mars Pathfinder flight rover, the 11 kg Sojourner vehicle shown to right. LSR, also a six-wheel rocker bogie design, introduces a *Volume Efficient Deployable Rigid Wheel* concept, as illustrated in the lower center inset. This composite/Al wheel design stows to about 30% operational volume and uses new 3D composite machined components.

If such Martian exploration is to be frequent and cost effective, there must be improved use of mass, volume, and power; an increased robustness and survivability of systems; and ultimately, on-board, task-adaptive autonomy beyond frequent telerobotic intervention of a human ground controller. In this paper we concentrate on the first issue, and to some degree the second – the development of improved mechanization approaches to Mars mobility and thermal isolation strategies for greater environmental robustness of enclosed electronic/computing/science instrumentation. What we report here illustrates several significant advances in planetary rover design, features of which should also impact design of terrestrial rovers, e.g. field reconnaissance vehicles:

- 30-40% reduction of mobility mass through use of composite versus metal construction, including introduction of complex 3D machined parts derived from a new JPL-developed resin transfer mold air lay-up carbon fiber process
- collapsible and actively articulated mobility structures that enable stowage of vehicles in as little as 20% of their deployed field operational volumes, as demonstrated in novel wheel and strut/joint geometrys
- an all-composite Warm Electronics Enclosure (WEE) design having improved thermal insulation, stabilization, and secondary power management (solar power generation and storage to interior rechargeable batteries) so as to eliminate need of RHU's (radioactive heating units) -- as enabled by use of a new opacified aerogel insulator in WEE walls, capacitive phase change material (PCM) in the WEE volume, and reduction of conductive feed-throughs to external rover interfaces
- combination of rover structure and thermal design into a composite chassis wherein the WEE -- as primary connection of the running gear elements and external science apparata – serves a dual, mass-reducing function (as well as eliminating the above noted 20-30% heat-loss associated with pass-through of a supporting Jeff-bar axle member)
- extension of Sojourner's coarse terrain map acquisition by structured (stripe) lighting, wherein now we use a novel diffraction grating projection of bright laser spots, their area-selective readout, and an iterative forward-looking ("pushbroom") geometric analysis to enable fast, reliable detection of terrain geometry and obstacles in the rover's path

In Section 2, we summarize the general features of the LSR-1 vehicle, contrasting them with JPL's recently flown Sojourner rover. In Section 3, we overview technical features of various LSR-1 subsystems – mobility, thermal, and sensing functions. Finally, in Section 4, we conclude by briefly describing our ongoing work on a related class of light vehicle, a Sample Retrieval Rover (SRR), whose development is targeted at demonstrating an approach to the planned NASA Mars sample return mission.

2. LIGHTWEIGHT SURVIVABLE ROVER (LSR-1)

LSR-1, **Figure 2**, was conceived as an approach to low mass, high mobility planetary roving in challenging thermal environments. Work began in fall 1995, and the vehicle configuration reported here was first demonstrated in ground field trails in fall 1996. The design is new, drawing as appropriate on Mars Pathfinder Sojourner [2] experience to retain flight legacy and relevance, but also introducing fundamentally different, novel materials and subsystem technology concepts. Common flight elements include:

- use of the Sojourner flight computing board-set (radiation-hardened 80c85) to provide a capability benchmark, and should there be reason, to facilitate rapid transition of the LSR design to flight readiness
- for similar reasons, development of LSR-1 obstacle detection and stereo imaging utilizing the Sojourner diode laser projection and CCD hardware implementation, with significant evolution to a novel "spot-pushbroom" imaging technique
- continued development of rocker-bogie mobility design, given its advantageous obstacle clearance/climbing performance (with an LSR-1 simplification to skid-steering versus Ackerman, so as to reduce actuator mass and drive requirements).

The areas of implementation in which LSR-1 significantly differs from design practice of Sojourner (and other rovers) are:

- development of a new concept for rover wheels (and subsequently the mobility running gear at large, cf. Section 4), the goal being to illustrate vehicle designs that can collapse for launch, rigidly deploy on operation, e.g., a future system that would stow to its approximate WEE footprint
- construction of many rover elements from novel 2D and 3D composites versus aerospace aluminum or steel, the objective being to reduce rover mass and improve structural interface thermal match (wrt. DCTE cycling fatigue at critical joins)
- introduction of a new thermal isolation concept supporting the all-composite, low mass rover design theme, the result being a warm electronics enclosure of improved thermal performance, better science volume at given mass, load-bearing integration of various mobility elements (rocker-bogie pivot cups) and science functions (front and rear instruments trays).

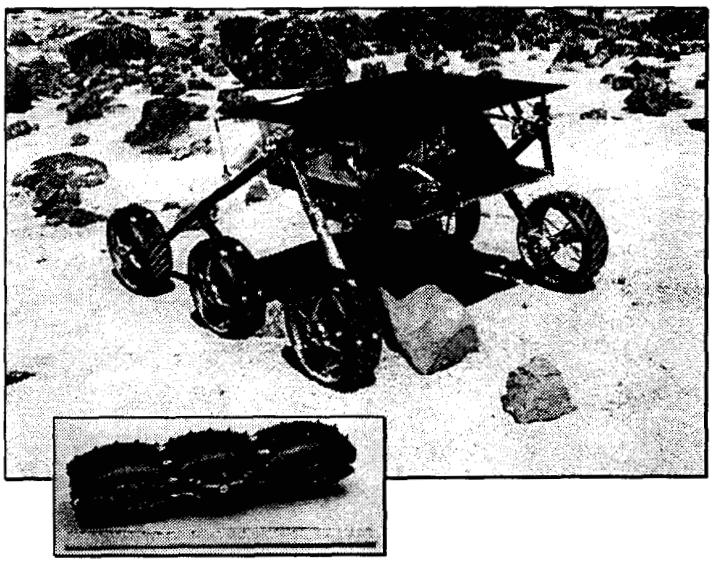

- 7 kg, six-wheel, rocker-bogie skid-steering LSR-1; vol. = 73x100x45 cm*3 (WLH) ~4x Sojourner (11+kg); 2D/3D composites + Al
- 21 cm dia. collapsible spoke wheel, NTR: "Volume Efficient Deployable Rigid Wheel;" total mobility system mass = 3kg
- .77 kg integrated thermal/structural sheet-and-spar WEE: 12 mil glass-epoxy walls, new opacified-aerogel/PCM controls, ~2x Sojourner volume, 80% mass, -40 to 0 °C
- laser diffracted spot projection with >95% direct sun CCD detection, no false alarms

OBJECTIVE: Develop, demonstrate, and evaluate for local area science sorties (e.g., Sojourner-class 10 meter dead-reckoned navigation) in simulated VL1/2 terrain, a new volume-efficient rover mobility design – ~20 cm wheel diameter, the collapsible wheel stowing to ~30% active volume – capable of 1-to-3 cm/sec traverse with visual hazard detection by hybrid spot-pushbroom laser/CCD-stereo sensor.

		Sojourner	*LSR-1*
Dimensions	Operational (h x l x w) Stowed	280 mm x 630 mm x 480 mm 72 liter (85 deployed)	447 mm x 1000 mm x 728 mm < 80 liter * (325 deployed)
Mobility	Type	6 wheel rocker-bogie Ackerman steering 6 wheel drive, 4 wheels steering	6 wheel rocker-bogie Skid steering 6 wheel drive
	Speed	0.4 m/min.	1.75 m/min.
	Wheel diameter	130 mm	210 mm
Ground clearance		130 mm	270 mm
Largest Obstacle		260 mm	350-400 mm *
Obstacle Avoidance System		2 CCD camera, 5 laser stripe projector	2 CCD camera, 2 laser spot projector
Warm Electronics Box Interior		218 mm x 283 mm x 123 mm	300 mm x 300mm x 150 mm
Thermal Control		25 mm silica aerogel, 3 W RHU	15 mm opacified aerogel, PCM panels*
Interior Temperature Range		-40 to 40 °C	-40 to 0 °C*
Power System		0.22 m2 GaAs solar array 150 W-hr primary Li Battery	0.25 m2 GaAs solar array* 30 W-hr rechargeable Li battery*
Computer		80c85	80c85, upgrade to rad-hard 32bit CPU
Telecommunications		UHF to Lander	UHF to Lander (or direct to Orbiter*)
Science		Alpha Proton X-ray Spectrometer	Multi-Spectral Imager, deployable tray, arm (gripper, μ-camera, etc.)
Weight		10.4 Kg plus 1.1 Kg science	6.5+ Kg plus up to 3.5 Kg science*

** Projections: will vary based on mission constraints and spacecraft/lander design*

Figure 2. Lightweight Survivable Rover (LSR-1) features and summary design parameters by comparison to Sojourner

3. LSR SUBSYSTEMS

The LSR primary subsystems reported here are mobility, thermal, and sensing. We present for each of these areas a pictorial summary of key results and accompanying text description of the underlying technical issues and design approach. The computing, power conditioning and sensor-referenced controls elements are similar to those of Sojourner, with our primary focus of the baseline LSR-1 design being mechanical subsystem and vehicle architecture integration. See also the recent work of Hayati et al. [3] on rover navigation & control, operator interface, and long range rover science field trials.

3.1 Mobility

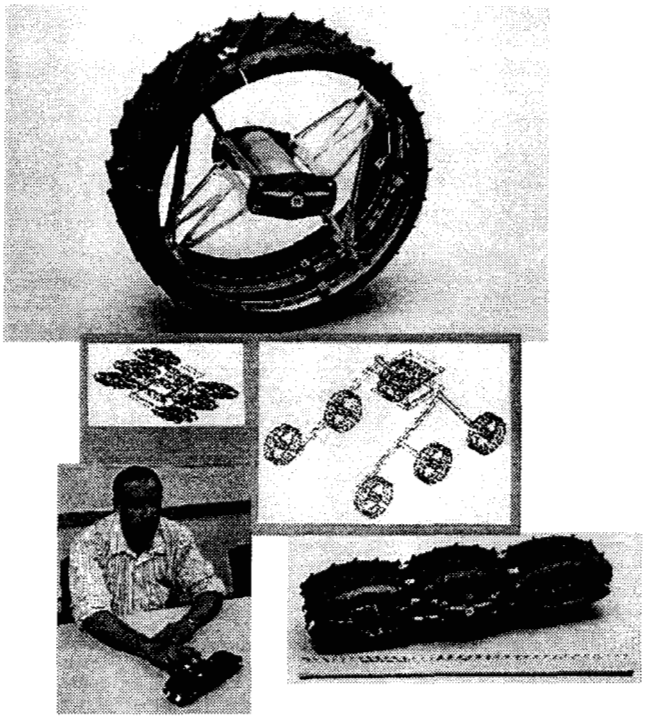

- Stowage efficiency motivated by spacecraft backshell geometry constraints (cf. Mars'98)
- Wheel rims are six-segment, four-ply 2D graphite polycyanate (+/- 45°) connected via four pin-ended spokes to central hub of thin-wall Al tube and 3D machined composites
- Self deployment (and locking) via pin-ended extension springs—deployed wheel volume ratio is 3:1, and total unactuated mass 260 g
- Kinematics is equal-spaced rocker-bogie linked by 2D composite struts/differential; joint segments, rocker cup and other load-bearing parts are new 3D RTM composite
- All rotating joints are Vespel SP-3, aromatic polyimide with 15% wt. moly-sulfide (est.10% mass savings over ball bearing pairs)
- Maxon motor/planetary gearhead actuation with 5th stage mods for increased torque

Figure 3. Summary of LSR-1 mobility subsystem development and key features

We begin with a brief empirical perspective on the evolution and use of the rocker-bogie geometry in LSR-1 design, and its Sojourner priors; we follow this with a technical description of the LSR-1 mobility components. (The historical lead-in is provided by D. Bickler): The General Motors Defense Research Laboratories facility in Santa Barbara, California, acting under contract to Jet Propulsion Laboratory of Caltech, developed a Surveyor Lunar Roving Vehicle (SLRV) during the 1960's. This work was led at GM by M.G. Bekker [4]. In addition to development of wheeled vehicles, this GM team also studied tracked vehicles and even developed some small concept models propelled by Archimedes' screws. GM ultimately developed to full scale a six-wheeled vehicle configuration (with six wheel drive) using three axles, one in each of three body sections, elastically articulated between them in order to conform to the terrain surface. This vehicle set records for its mobility and established a baseline kinematics concept for future developments. SLRV was 1.8 m long and used 46 cm diameter wheels. With a coefficient of friction of 0.7 (usual for rocks, etc.), the SLRV could climb a square vertical step of 69 cm in height -- a one and one-half wheel diameter sized step or comparably, a three-eighths vehicle length sized step (one analogy being a 5.3 m long passenger car climbing a 2 m step!).

Planetary rover research resumed at JPL in the early 1980's, and again all vehicle types were considered. While advances in the field of robotics made legged vehicles an interesting option, their inherent complexity and computational requirements impeded practical development of lightweight, reliable interplanetary explorers. Tracked vehicles (especially well-suited for snow and mud) were evaluated again, and sometimes observed to "throw a track" when a rock became entrained between the track and drive wheel. Large, powerful vehicles (military tanks) can crush sizable entrained rocks; however, smaller vehicles such as an envisioned

one meter tracked Mars rover were thought unlikely to crush the smallest of stones. When all such factors were considered, JPL elected to pursue wheeled rover designs, leaving the number wheels a variable design parameter. It is generally observed when a sequential wheeled vehicle climbs an obstacle, the more wheels driving forward against and over the obstacle, the better the climb performance. Six-wheeled vehicles have a decided advantage over four-wheeled vehicles; and, eight wheels are generally a system complexity trade beyond their advantage. Weight and friction of additional wheel drive mechanisms (in all wheel drive) is not worth the gain in mobility, and steering an eight wheeled vehicle is often a difficult task. Further, disadvantages ensue if six wheels are connected in pairs by axles. Most important, the ground clearance is impaired, but perhaps equally significant, wheels tied by axles tend to twist and slide sideways when one wheel is raised significantly. Mathematical analysis based on idealized models was used to optimize designs and design trades on various wheeled mobility options. Two types of obstacles were analyzed : "bumps" and "steps." Bumps fit between the axles while steps raise the vehicle up onto a mesa. Bumps were viewed as more important on Mars due to the many individual rocks its a relatively flat surface, and as it turns out, are more difficult for the vehicle (although steps sometimes appear more spectacular in demonstrations). The Surveyor Lunar Roving Vehicle did not fare well over bumps, had poor ground clearance, and often hung ("trapped") on obstacles between the wheels. Analysis of the bump problem shows that elastic suspension systems suffer an inherent difficulty: As the elastically suspended wheel (one with springs supporting it) climbs an obstacle, the downward force is increased due to the rate of the spring deflection. Correspondingly, the other wheels working to drive against the obstacle and increase friction for climbing, have their downward force reduced making it easier for them to slip. For this reason, JPL devised suspension linkages which do not use elastic elements. The result is the JPL six-wheel rocker-bogie which has been explicitly designed to exploit wheel torque reactions and obstacle reaction forces [5].

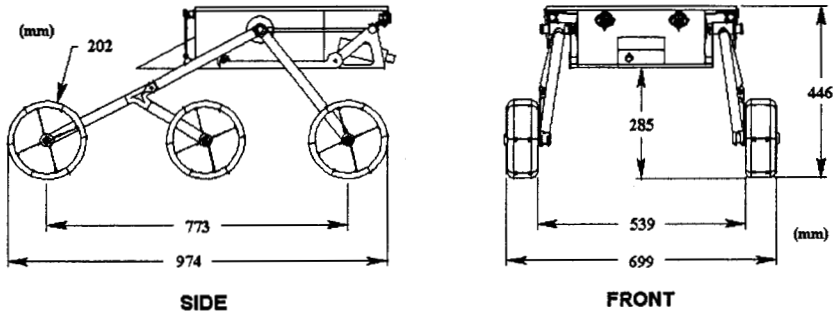

LSR-1 uses 1:1 spaced rocker-bogie design with 20 cm wheels to implement a 3 Kg mobility platform of ~80 cm wheelbase. In early ground trials ("MarsYard" operations in Viking Lander 1, nominal and VL2 site rock distributions of ~ 6, 8-9, and 17-18% areal occupancies) LSR-1 displays excellent terrain performance, surmounting VL2 obstacles of nearly twice wheel diameter; average ground pressure of <800 Pascal (0.12 psi) at tire/soil interfaces insures excellent flotation in loose sand (Army tank figures are ~ 69,000 P).

Figure 4. Dimensioned drawing of LSR-1 side and front views

A "Volume Efficient Deployable Rigid Wheel [6]," has been developed (cf. L. Sword with collapsed wheel in **Figure 3** above) to enable stowage of "large" rovers in relatively "small" spaces. This wheel has six rigid segments hinged together that form a "tire". The tire is then connected to the central hub via four pin-ended spokes. Deployment force and locking are derived from a pair of pin-ended extension springs. The tire is made from 4 ply of graphite-epoxy 2D composite oriented to plus and minus 45 degrees. Circumferential strength and stiffness are achieved through machined aluminum reinforcement ribs which also provide the hinges and pivot points for the spokes. The central hub is fabricated from a thin-walled aluminum tube "capped" with end fittings made from a new JPL 3D composite material [7]. The wheel is self deploying, (i.e., no actuator is needed), requiring only a release of mechanical restraints. The deployed wheel volume is approximately 300% that of stowage. Future VEDRW iterations investigate forming cleats/growsers as integral tire elements rather than adhesively bonded components, also capping the tire body with more environmentally resistant materials. We discuss this briefly in Section 4 as pertains to our development of the new Sample Retrieval Rover. The VEDRW deployment/locking springs could be made from square wire resulting in a smaller and less massive spring with the same compressive load capability. The total mass of this first prototype 20 cm diameter deployable wheel is 260 g.

LSR-1 is a testbed for innovative applications of polymeric and composite materials. All rotating joints on LSR-1 have been designed and built using Vespel SP-3 bushings rather than the traditional ball bearing pairs (as used in the MPF/Sojourner flight rover). Vespel SP-3 is an aromatic polyimide filled (15% weight) with molybdenum disulfide. When properly used as a bushing, this material provides a low friction, wear resistant joint, usable in a vacuum and extreme temperature environments. This approach is estimated to have reduced the mass of the 3 Kg mobility subsystem by over 700 g or equivalently 10% of the total rover mass! As noted earlier, use of traditional 2-D composites and a new 3-D composite being developed at JPL provide some further 20-40% mass saving in mobility struts and joints. See reference [8] for a discussion of the composite forming processes.

3.2 Thermal Controls/Chassis

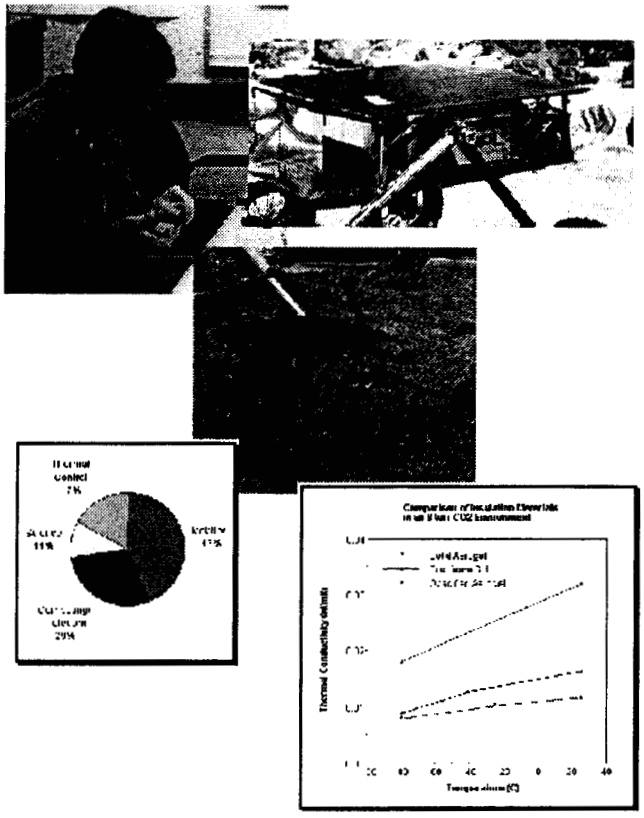

- Warm Electronics Enclosure (WEE) is both a thermal control and structural member – rigid sheet-and-spar 12 mil glass-epoxy, 1.5 cm thick wall 15x33x33 $(cm)^3$ box construction carrying front deployable and fixed rear trays
- Relatively little advance in Mars-relevant insulators between Viking and MPF missions (difficult thermal design regime of 1-50 Torr)
- LSR-1 insulation is new opacified aerogel of 10-30% lower thermal conductivity--compare to MPF lander foam & MFEX solid aerogel, per simulated 8 Torr CO_2 environments
- Diurnal cycling/heat loss effects are better stabilized through use of Phase Change Material (PCM) upper/lower panels, each having transition temp. of -10°C and 4 Kcal thermal capacitance
- External pivot cups eliminate the MFEX internal Jeff-tube pass-through -- a major heat loss source – as are also cabling ports

Figure 5. Summary of LSR-1 thermal control subsystem development and key features

Future small Mars rovers will have limiting constraints on total mass, stowage volume and power availability. As a general system objective, it is desired that a greater percentage of rover mass and volume be allocated to science payload (25-50%). Operational goals are stated in terms of many months or even years, with science site latitudes as high as +/- 75 degrees envisioned (near polar temperatures, ranging to -100°C). Finally, it is still debated if such systems (if any) will carry RHU's to provide heating of interior electronics, as has been past practice. Taken together, these considerations argue for minimizing thermal losses, mass, and non-functional volume of isolating thermal enclosures, as well as developing optimal solar power collection and high energy density, low temperature secondary (rechargeable) power sources. As a corollary, rover mechanical design approaches which more tightly integrate mobility and thermal functions – e.g., make dual functional use of common structural elements and eliminate mutually compromising requirements – are important. The LSR-1 Warm Electronics Enclosure [9, 11, 12] reported here addresses thermal/ structural design goals, and related work on new low-temperature Li batteries [1] will provide secondary power sources enabling lower ambient temperature operations. For the long term goal, it is possible to envision rovers without volume and system design constraints imposed by a unit-body WEE architecture; however, this will require significant advance in low-temperature electronics and distributed thermal controls (serendipitously integrated throughout other functional elements of the rover system).

The 10 torr CO_2 Mars environment falls in a transition thermal regime – not well studied -- between the continuum (50 torr and above) and the Knudsen free molecular conduction (1 torr and below). There has been a limited evaluation of insulation materials for Mars environments. Wilbert, et al. [10] conducted a study for Viking that evaluated foam insulations, fibrous, powders and multi-layer insulation (MLI) for thermal control. The outcome was primary use of several inches of foam insulation and some MLI on the Viking Landers. Other studies of that time period assumed a foam insulation of 3 to 4 inches thick [Nagel; Tracey, 10]. A more recent study revisited the issue of Mars thermal control and evaluated additional porous foam insulations [Fischer, 10]. This bulky and mass intensive design approach has continued for the Pathfinder (MPF) lander, which uses 2 inches of 50 mg/cc foam enclosed in a composite honeycomb shell. All these systems or studies consider stationary landers having neither the mass or volume limitations that rovers do. The Sojourner over design was the first system to fully consider the unique physical constraints

of the Martian environment. That task studied foams, vacuum jacketed enclosures, opacified powders, before settling on the use of 15 to 20 mg/cc monolithic silica aerogel for thermal control [Hickey '95, 11]. This use of aerogel specifically addresses transition-regime thermal control as follows: The effective thermal conductance of an insulative system consists of two components, the solid conductance-radiative conductance (independent of pressure) and the convective component. Gas conductance depends on the mobility inside the voids of a material, and is governed by the relative dimensions and connectivity of the open volume and the gas mean free path. If the interstitial space between material (whether they be voids, particles or fibers), becomes smaller than the mean free path of the gas within the insulation, then the mechanism for gas transport shifts from the continuum regime to free molecular conduction in the Knudsen regime. (The mean free path of a gas being inversely proportional to the gas pressure). For CO_2 at 10 torr, the mean free path is approximately 3 to 5 microns in the temperature range from - 90°C to 25°C. Solid aerogel has pore dimensions 6 to 11 nanometers. This means that the effective gas conduction within the aerogel is a fraction of value in the continuum regime, and is dominated by the conductive-radiative component of the silica aerogel structure. Since low density aerogels approaches 80 to 90% open cells, direct conductance is minimized. Because of the high void fraction and the resulting low mechanical properties of low density aerogels, a lightweight supporting structure has to be designed and integrated into the thermal control [9]. Hickey, pictured in **Figure 5** above, pioneered and implemented the first such baseline approach [Hickey '95, 11] for Sojourner. To that design problem is now added the need for ultra-low mass (viz. thin-wall/low-volume) heat storage and diurnal cycle compensation in the face of thermal control without RHU's [Hickey '96, 11]. Recent work at JPL by Hickey, Manvi and Knowles [12] investigated the use of Phase Change Materials (PCM) for WEE thermal energy storage and demonstrated reproducibility of PCM panels applicable for use in the temperature range of Mars environments.

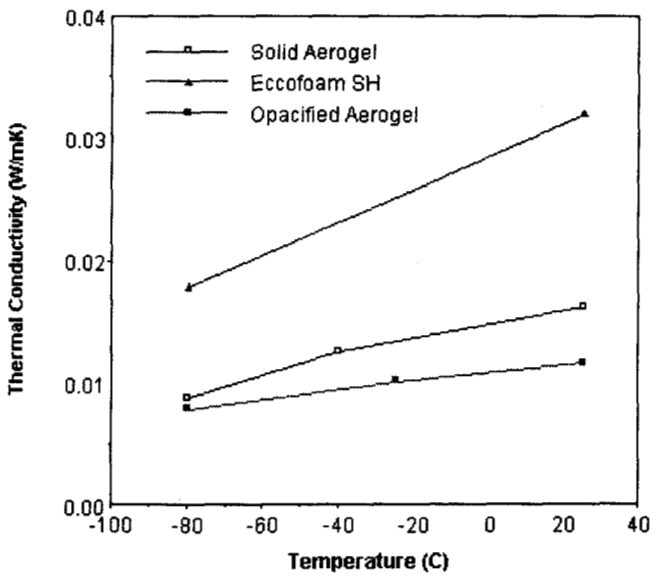

LSR-1 development took the Sojourner WEE as a baseline, and then advanced both thermal and structural design features. Thermal losses were minimized by two significant changes. The first was introduction of an isolating opacified aerogel having 10-to-30% lower effective thermal conductivity in a simulated Martain 8 torr CO_2 atmosphere as compared to the Pathfinder rover design. This is illustrated in **Figure 6** which compares the silica aerogel used in Sojourner, a conventional low conductivity foam insulation used in the related Mars Pathfinder lander, and the opacified aerogel being developed for the LSR. This lower conductance insulator enabled LSR-1 WEE wall thickness to be reduced from 25 mm to 15 while retaining the same effective thermal isolation capability. A second major change from Sojourner design was to directly attach the rocker-bogie mobility system to the external thermal chassis walls, rather than using an axial tube passing through the walls. This change reduces rover mass and eliminates a source of major heat loss observed in Sojourner tests. From a functional point of view, the WEE now becomes an integrated thermal/structural member, including attached science trays.

Figure 6. Comparative thermal conductivity of candidate WEE wall insulation materials

Reference [8] overviews our recent development of 2D and 3D composites for use in robotic arms and rovers. We note here a few summary and concluding points regarding the LSR-1 structural implementation and WEE design. The integrated thermal/structural chassis is a lightweight sheet-and-spar 12 mil thickness glass epoxy assembly that has isolating aerogel integrated within its walls. This is a low thermal loss 15x33x33 cm^3 (exterior volume) 1.5 wall thickness design that also provides a rigid, high-stiffness structure member. This design achieves about two times the Sojourner interior isolated volume at similar mass (after one discounts weight savings of Jeff-bar elimination), in addition to realizing its integrated structural functions. Included within this mass budget are two interior PCM panels developed in cooperation with Energy Sciences Laboratories, Inc. (ESLI). These two panels have an 7% increase in PCM mass fraction (73% current vs. 65% previous) over previous such panels and are covered with a carbon fiber flock coating having emissivity greater than 0.95. The PCM panels act as heat storage elements which maintain more uniform internal temperatures during typical diurnal cycling [12]. Experimental tests to date indicate that the LSR-1 WEE design will (with secondary power management using similar gross power budgeting as Sojourner) maintain -40-to-0°C interior temperatures [9; Hickey'96, 11] by contrast to -40-to-40°C variation observed in comparable Sojourner tests.

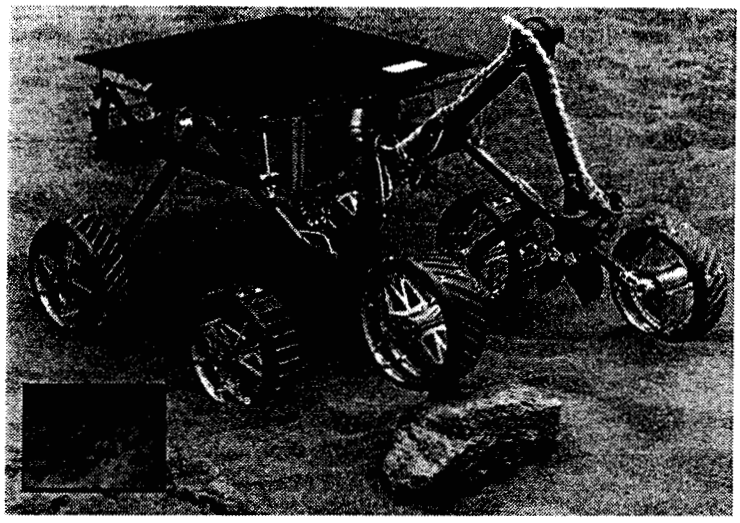

With regard to other composite assemblies of LSR-1, we use graphite-polycyanate 2D composite laminates to fabricate science trays, rocker-bogie struts, associated differential bar, and the collapsible wheel rim segments. The properties of such 2D materials are reasonably well understood for space environmental application, and we are now conducting some further comparative tests with respect to temperature and radiation dependent mechanical behaviors. As noted earlier, we have developed a new 3D graphite-epoxy composite [8] that can be machined-and-tapped to form intricate parts. We fabricated LSR-1 running gear joint segments, wheel hubs and other major stress-bearing areas of this new material, which has a density about half that of aluminum alloys, and competitive mechanical design properties. In addition to its inherent mass savings, use of a properly tuned composite design potentially reduces thermal DCTE mismatch at joins.

Figure 7. LSR-1 rear left view (MicroArm-1 replaces rear science tray) as equipped to perform sample acquisition, close-up viewing and fresh rock exposures; inset is sample rock data acquired by multispectral imager (front tray)

We have also recently developed and demonstrated all-composite, lightweight robot arms from similar 2D (links) and 3D (joints) materials [8]; these robotic developments include a class of small dexterous sampling and sample cache/return processing arms for use with light rovers [13]. One such device is illustrated in **Figure 7**: *MicroArm-1* is a .7 meter long, 1 Kg 3-d.o.f.. torso-shoulder-elbow (roll/pitch/pitch) configuration with additional end-arm pitch degree of freedom and clamshell scoop in the effector. The effector integrates a micro-camera and powered rock abrasion tool, and is actuated in all joints by novel, high power density rotary piezoelectric motors [14]. This view of LSR-1 shows the rear composite differential bar acting to distribute left back wheel forces experienced in rock climbing; one can also see, looking from left rear of the WEE forward, an integral actively deployed front science tray, which carries a .3 Kg multispectral imager plus imaging photo-spectrometer (designed and developed by B. Wilcox).

3.3 Sensing of Terrain and Hazard Avoidance

Planetary rovers must be able to accurately, quickly, and reliably characterize terrain before them. Several active and passive technologies are available for such tasks, including IR proximity detectors, "laser radar," stereo vision and structured light. In the case of rovers embarking to other planets, the rigors of space travel and the target planet's environment must be considered. Fragile moving parts like the nodding mirror of a laser radar might not survive the G-forces of atmospheric entry and landing. In the case of Mars, computing power is another important consideration. Radiation hardening and flight certification, for instance, restricted the Mars Pathfinder Sojourner rover to an 8085-class CPU. This impacts the processing power available for all tasks including vision. In this context, many stereo vision approaches have proved too costly or computationally impractical (in m/v/p budget) to provide safe, rapid rover motion. The LSR-1 sensing subsystem is derived from the IR diode laser light striping and stereo CCD imaging hazard detection subsystem recently flown on Mars Pathfinder Sojourner [2]. Several of the same flight-qualified components are incorporated into LSR-1. The intent has been to develop an improved capability that reduces compute time, increases hazard detection confidence, and if desired, would quickly transition to flight application with known benchmarks.

Sojourner uses a stripe-based structured light system wherein five small lasers project stripes onto the terrain imaged by the rover's two cameras. Two images are taken for each hazard scan: one with the lasers turned off and one with them on. The difference between the two images reveals the stripes on the terrain. The laser and camera are arranged so that the height of the terrain relative to the rover can be determined using simple geometry once the stripes are located. The Pathfinder system is reliable and accurate. It is also fast compared to general stereo vision approaches since the computational requirements are significantly lower. There are, however, at least two possible avenues for improvement. First, image differencing is time consuming since image acquisition on a 8085-based system is slow. Second, the Pathfinder algorithm does not make full use of information available to it. It does not account for lens distortion, nor does it compute the 3-dimensional coordinates of terrain illuminated by the lasers. More detailed and precise information could provide for more efficient navigation.

Our generalized hazard detection concept, as summarized in **Figure 8** below, has to date been integrated into two rovers: Light-weight Survivable Rover (LSR-1) and Rocky 3 (an earlier JPL microrover ground development system prototype for Sojourner).

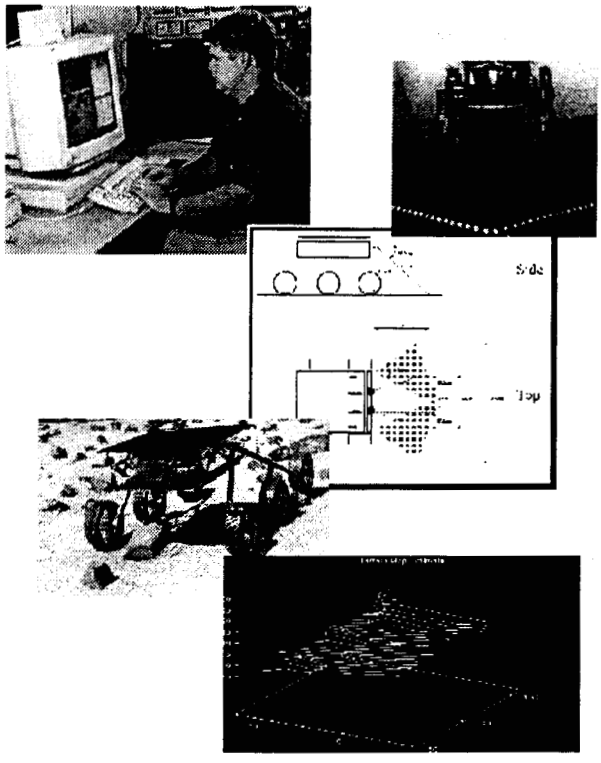

- Sojourner/MPF employs five laser stripe projectors and difference imaging to estimate frontal, non-rectilinear array of terrain slopes
- LSR introduces a new spot-pushbroom hazard detection scheme -- diffracted projection of many (10-to-15) intense spots from a well collimated laser into a uniform cross field array, and direct image detection
- Significant benefits include much improved ROC (e.g., >97% detection in direct sunlight, MarsYard, zero false alarms) , and reduced computation/power requirements
- Tests in LSR-1 (80c85 MPF CPU)/Rocky 3 (486 upgrade) imply 5-to-20X speed-up of Sojourner computations, with concomitant increases in driving speed up to 6 cm/sec
- Provides basis, per simulation at left, for highly efficient, continuously-update forward terrain map estimate, and robust navigation over diverse surfaces

Figure 8. Summary features of generalized spot-pushbroom hazard detection scheme developed for LSR-1. Upper right picture (Rocky 3) illustrates the diffracted spot pattern emanating from two laser diode collimated projectors. Bottom plot shows a recovered terrain map from experimentally simulated continuous terrain navigation (approx. 1 cm accuracy at 50 cm)

Both robots utilize a six-wheeled rocker-bogie suspension like that of MPF/Sojourner. LSR-1, as reported here, is equipped with an engineering model 80c85 boardset developed for Pathfinder; Rocky 3 uses a 486-based commercial computer. The requirement for image differencing on Sojourner is primarily due to optical limitations. There is not enough projected laser stripe intensity to enable direct detection in sunlight without image differencing (threshold comparison of stripe-on/stripe-off background imagery).

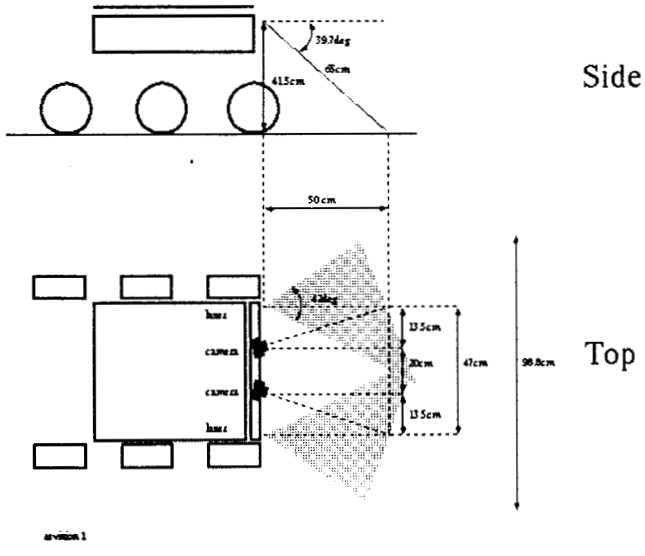

The new LSR-1 approach also uses laser illumination of similar input power, but now discrete spots are projected rather than a continuous, highly distributed line (stripe) image. As observed at an individual CCD pixel, spots are several hundred times improved in brightness over stripes. Additionally, full 3D information, with compensation for camera distortion, can be computed by geometric reconstruction for the spot-imaged terrain -- wherein the projected spot array can be progressively advanced in a pushbroom fashion – hence, a *spot-pushbroom* sensor modality.

To meet performance goals for LSR-1 hazard detection, the camera system must image laser spots at a nominal range of 0.65m in full sun. A key factor regarding spot detectability is the ratio of spot brightness to reflected sunlight in the image. We maximize the spot/ambient ratio in two ways: first by using a laser whose wavelength (860nm) is in a region where solar power is low; and second, by filtering the reflected light to a narrow band around that wavelength before the scene is imaged.

Figure 9. Sketch of LSR-1 imaging geometry for spot projection and geometric reconstruction

LSR-1 hazard detection is composed of two camera/laser pairs, arranged as in **Figure 9**, above. For now, consider one of the pairs by itself. First, laser light is split into 15 co-planar beams with the central beam aimed at the ground in front of the rover (about half a meter for LSR-1). The rest of the beams fan out to the left and right. On flat terrain, the beams form a straight line of spots. If an obstruction is present, they follow its contour instead. The spots are imaged by a camera offset horizontally from the laser at the same height above the ground. On-board software finds the spots in the image which are in turn used to determine coordinates of the terrain. From the camera's point of view, each spot shifts left or right depending on the height of the obstacle the corresponding beam strikes. Geometrically, the approach is analogous to ranging with a stereo camera pair, except one of the "cameras" is a laser. In traditional stereo vision systems, the range to objects in a scene are computed based on disparity between the two cameras' images at each pixel. In this imaging system, however, the disparity is computed between where a laser spot should appear if the rover were on flat ground and where it is actually detected. An overview of the calculation follows [15]: Assume for now that a linear equation for each laser beam is known, and that one particular beam is under consideration. As it strikes the ground, the beam forms a bright spot in the image. The centroid of the bright spot is computed in pixel coordinates on the camera's imaging array. Next, an equation for the ray moving from the pixel out the lens is computed. The intersection of the ray with the equation for the beam is the location of the surface of the terrain.

The remaining issue is how to differentiate the 15 spot beams. Fortunately, the system geometry provides a convenient solution. Since the laser and camera are positioned at the same height, each beam always appears on the same scanline, assuming linear camera optics. If the plane of the beams is tilted slightly each beam will appear on a separate scanline. The beams may then be found unambiguously, by scanline. Furthermore, the knowledge that each beam will only ever appear on a specific scanline may be used to reduce the image processing necessary to find the beams. Equations for each beam are computed ahead of time in a calibration phase (The optics of the camera are modeled using an earlier JPL-developed approach of Yakimovsky and Cunningham with an extension providing for radial distortion developed by Gennery, cf. reference [15, ICRA'96] and further citations therein. The camera model provides for the computation of a ray from any pixel out the lens).

We conclude this sub-section with brief summary of hazard detection performance in initial tests; see also reference [15]. Overall speed of the system depends primarily the time required to collect images of the projected laser spots. Since the system uses simple thresholding to find the spots, image processing time for this function is negligible. On the 80486-equipped Rocky 3 test vehicle, image acquisition takes about 300ms; the 80c85-based LSR-1 baseline system requires 1 to 4 seconds. It is anticipated that the system can complete over 3 scans per second for 486-class CPUs, but will be limited to about 0.3hz on 8085-class systems. While simple thresholding to detect projected spots affords good processing speed, the approach must be reliable to be useful. A detailed analysis of the optical system being prepared for publication shows that the spots will appear at least 5 times as bright as the nominal terrain in an image. This 5 to 1 signal-to-noise ratio should provide reliable spot detection in full sun.

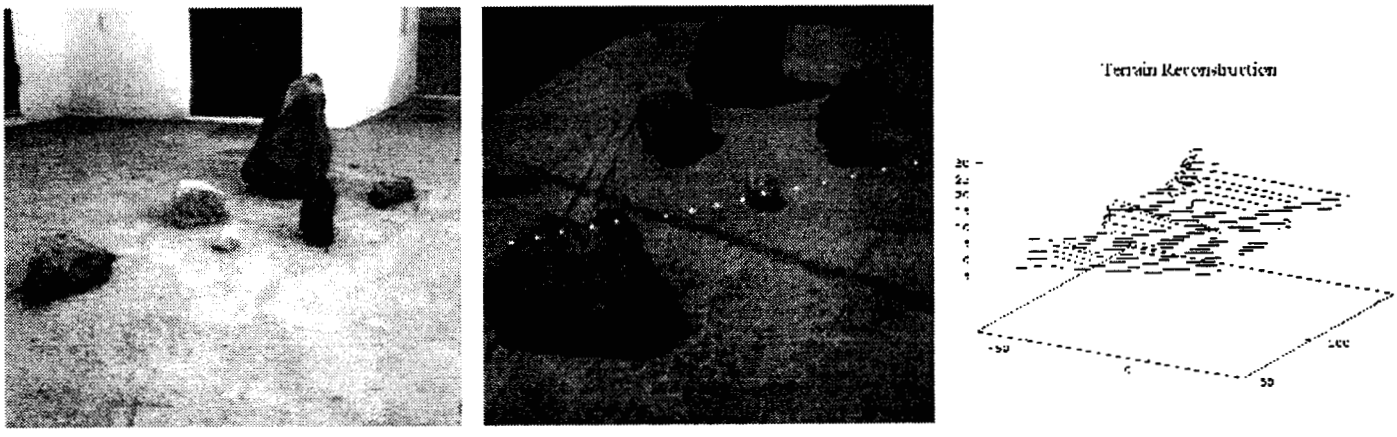

Figure 10. Test imagery (full sun), example of IR spot projection (with filtering), and reconstructed terrain sweep

An initial experiment for determining the operational reliability and accuracy of the approach was conducted by moving the sensor across a small patch of simulated Mars terrain. A series of 24 images were taken as the sensor was moved across. The reported height for each rock was found to be within 1 cm of the true height. Accuracy in the lateral and fore-aft dimensions was evaluated qualitatively by inspecting a reconstruction of the scene generated using the sensor data. Every hazard was detected, and no false obstructions were reported. Greater than 95% of the detectable laser spots were found using simple thresholding.

We have applied the above LSR-1 hazard avoidance implementation to short range sorties in the JPL MarsYard (per earlier description, an outdoor facility that faithfully recreates rock area/terrain densities as known from models of the Viking lander flight 1 and 2 landing sites). This is depicted in Figure 2. As with Sojourner, LSR-1's 80c85 computing implementation enables a stop-and-stare mode of obstacle detection: The reconstructed spot beam projection is analyzed for rocks within the vehicle path and according to preset limits of vertical clearance and/or tangent angle avoidance, and the vehicle proceeds (about a ¼ wheel turn in current practice). If a detected feature is judged an obstacle, then a skid-steered turn is executed with dead-reckoned course maintained by onboard engineering sensors (gyro and accelerometers). Under optimal conditions, LSR-1 is estimated to have about 4-5x Sojourner's averaged .7 cm/sec ground speed, as facilitated by the more selective areal scan/detection of the spot based imagery. At conclusion of the sortie on designated vector/distance, the LSR-1 executes Sojourner's analogous "find-rock" function wherein the steering system now centers on the detected "science objective," lowers its science tray with imaging camera, rolls to contact (as detected by a limit switch) and acquires imaged science data per Figure 7 example.

In summary, the new LSR-1 hazard detection and terrain mapping sensor concept provides reliable hazard detection several times as fast as current MPF/Sojourner technology, as benchmarked against identical flight computational resources. Initial results point to several potential improvements: First, image acquisition is a primary bottleneck in the current system. Nearly all time between hazard computations is devoted to collecting images of the laser spots. This could be improved significantly with a faster flight processor or new imaging technology, or both. Second, reliability of spot detection could be further improved through use of more narrow bandpass filters in the camera optics. (The requirement to detect far off-axis has so far precluded use of common interference filters, but a redesign of the camera optics might so allow). In general, we note that flight qualified real-time vision and associated fast terrain navigation planning functions remain important and as yet un-addressed requirements for longer range rover missions, and/or those computationally bounded applications where high rates (10's to 100's cm/sec) of ground speed are needed to meet mission timeline constraints.

4. ONGOING WORK

In closing, we briefly note our progress toward development of another light rover concept for Mars application. The problem motivating this work is *Mars sample return*. In this theater of operation, it is assumed a prior mission has conducted areal science surveys with a long range rover(s) and collected ("cached") samples of interest. The earlier mission will possibly leave markers/ beacons to guide precision landing; the "science rover" will likely itself carry a beaconing cache, which on arrival of the return mission provides a directional target for the sample retrieval rover and its short range navigation for cache pick-up. The sample cache pick-up scenario presumes a minimum duration visit to Mars, perhaps collecting a cache in as little as one day, and returning soonest (after appropriate planetary protection containment processing at the return lift-off site). Most landed resources will be devoted to the return/ascent mission phase, and it imperative that the sample return rover economize in mass/volume. To this end, we have undertaken development of a fast, small, fully collapsible Sample Retrieval Rover (SRR) R&D prototype.

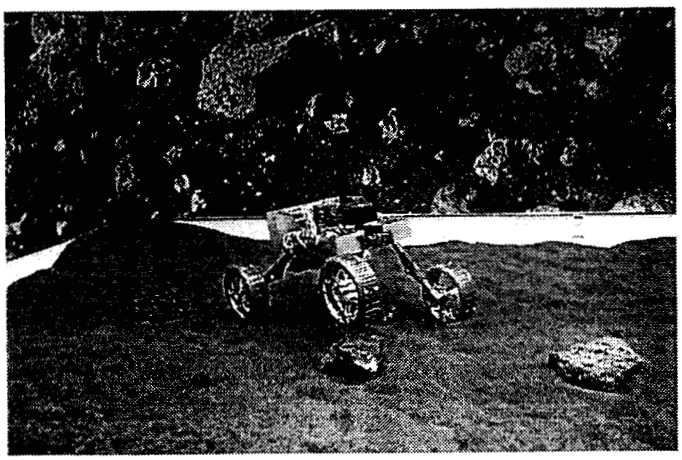

Operation of SRR during the sample cache retrieval event is broken down into a sequence of navigational and sample cache localization acquisition phases, which in simplest form might be:

- open terrain navigation to cache area (dead-reckoned)
- mid-range beaconing guidance into the cache site
- visual localization of the cache site (e.g., science rover)
- terminal guidance of SRR onto pick-up approach vector
- visual acquisition of cache and mechanical pick-up
- return to Ascent Vehicle and cache hand-off

This sequence is meant as illustrative, rather than a mission flow. Each phase is in practice functionally somewhat overlapping, but should make clear the distinct sensing and control requirements.

Figure 11. Sample Retrieval Rover in JPL Planetary Robotics Lab test pit (SRR top cover removed, and 3-d.o.f sample cache arm assembly complete only to first link and its elbow-mounted goal acquisition camera)

The SRR vehicle extends the LSR-1 architectural features and capabilities in several distinct directions:

- implements fully collapsible mobility, wherein running gear struts break over at their mid-points and positively deploy under mechanical stored energy from restraint -- as with LSR-1, the wheels are self-deploying, and augmented with hardened spring steel growsers and Kevlar-surfaced wheel rims
- articulates the four-wheel bogie axle by a active split drive differential, which enables difference stances to be implemented, as best suited to current vehicle function -- e.g., running fast and low over flat terrain, elevating for clearance of an obstacle, getting in a "squat pose" for best leverage in lifting with arm extended, etc.
- utilizes PC104-based 80486 computing architecture, enabling exploration of various fast sensing and control algorithms likely to be supportable in next generation 32 bit flight hardware -- stereo depth mapping, cache localization by image correlation, inverse kinematics control for visually referenced arm positioning, etc.

ACKNOWLEDGEMENTS

This work was carried out at the Jet Propulsion Laboratory, California Institute of Technology, under a contract with the National Aeronautics and Space Administration. We gratefully acknowledge support of the NASA Telerobotics Program for this research. Areas of cognizance for the above reported work are: P. Schenker, PI; L. Sword, mobility; G. Hickey, thermal controls & materials; L. Matthies, sensing & hazard avoidance; E. Baumgartner, system engineering & integration (SRR); B. Wilcox, on-board computing & control; H. Aghazarian, software development & user interfaces. Tucker Balch, currently a Ph. D. student at Georgia Institute of Technology, performed portions of the algorithm development and experimental data collection reported in Section 3.3 during a summer 1996 JPL visiting appointment.

REFERENCES

1. C. R. Weisbin, D. Lavery, and G. Rodriguez, "Robotics technology for planetary missions into the 21st century," Proc. 1997 Intl. Conf. on Mobile Planetary Robots, Santa Monica, CA, January 29-31 (ref: Planetary Society, Pasadena, CA, Org: L. Friedman), and, D. L. Shirley and J. R. Matijevic, "Mars rovers: past, present, and future," Proc. Princeton Space Studies Inst. 20th Anniversary Conf., May, 1997; see also, http://robotics.jpl.nasa.gov, and link therein to Rover and Telerobotics Program Overview (Mars technologies).
2. The Rover Team [D. L. Shirley at al.], "The Pathfinder Microrover," Journal of Geophysical Research, Vol. 102, No. E2, pp. 3989-4001, Feb. 25, 1997; see also http://www.jpl.nasa.gov [ref: Mars Pathfinder Mission, Sojourner Rover].
3. S. Hayati, R. Volpe, P. Backes, J. Balaram, R. Welch, R. Ivlev, G. Tharp, S. Peters, T. Ohm, R. Petras, and S. Laubach, "The Rocky 7 rover: a Mars sciencecraft prototype," Proc. 1997 Intl. IEEE Conf. on Robotics and Automation, Albuquerque, NM, April 20-25; and, P. G. Backes and G. Tharp, "The WEB interface for telescience (WITS)," ibid.; see also, R. Volpe, J. Balaram, T. Ohm, and R. Ivlev, "The Rocky 7 Mars rover prototype," Proc. IEEE/RSJ International Conf. on Intelligent Robots and Systems (IROS '96), Osaka, Japan, November 4-8, 1996, and citations therein.
4. M. G. Bekker, Introduction to Terrain-Vehicle Systems-Part 1: The Terrain, Part II: The Vehicle, University of Michigan Press, Ann Arbor, Michigan, 1969.
5. D. Bickler, "Articulated Suspension System," U.S. Patent Number 4,840,394, U.S.Patent Office, Washington, D.C., 1989; D. B. Bickler, "Computing true traction forces on an eccentrically loaded vehicle," SAE Technical Paper Series, Paper Number 901657, Society of Automotive Engineers, Warrendale, Pennsylvania, 1990; and D. Bickler, "A new family of planetary vehicles," Proc. Intl. Symp. on Missions, Technologies, and Design of Planetary Mobile Vehicles, pp. 301-306, Toulouse, France, September 28-30, 1992.
6. L. F. Sword, G. D. Harvey, and J. A. Frazier, "Deployable rigid wheel," NASA Tech Briefs, June, 1997, ref: NPO-19982.
7. D. K. Brown, "Near isotropic, machinable, resin transfer molded composite," filed as NPO-19918, Jet Propulsion Laboratory, Caltech, Pasadena, CA, May, 1996.

8. P. S. Schenker, Y. Bar-Cohen, D. K. Brown, R. A. Lindemann, M. S. Garrett, E. T. Baumgartner, S. Lee, S.-S. Lih and B. Joffe, "A composite manipulator utilizing rotary piezoelectric motors: new robotic technologies for Mars in-situ planetary science," in Enabling Technologies: Smart Structures and Integrated Systems, SPIE Proc. 3041, San Diego, CA, March, 1997.

9. G. S. Hickey, D. E. Braun, P. Tsou, D. K. Brown, W. H. Mateer II, and W. Han, "Lightweight, thermally insulating structural panels," NASA Tech Briefs, May, 1997, ref.: NPO-19504.

10. O. J. Wilbers, B. J. Schelden, and J. C. Conti, "Martian soft lander insulation study," in Heat Transfer and Spacecraft Thermal Control, Progress in Astronautics and Aeronautics, Vol. 24, pp. 630-658, January, 1970; R. Nagel, "Thermal control aspects of a stationary Martian surface laboratory," Proc. AIAA 3rd Thermophysics Conference, Los Angeles, CA, June, 1968; T. Tracey and T. Morey, "Mars lander thermal control system parametric studies," Proc. AIAA 4th Thermophysics Conference, San Francisco CA, June 1969; and, W. P. Fischer, W. Ebeling, B. Hass, and K Keller, "Porous insulation performance under Mars Environment," Proc. SAE 23rd Int. Conference on Environmental Systems, Colorado Springs CO, July, 1993.

11. G. S. Hickey, D. Braun, L. C. Wen, and H. J. Eisen, "Integrated lightweight structure and thermal insulation for Mars rover," Proc. SAE 25th International Conference on Environmental Systems, San Diego, July, 1995; G. Hickey, D. Braun, L.C. Wen, and H. Eisen, "Integrated thermal control and qualification of the Mars rover," Proc. SAE 26th International Conference on Environmental Systems, Monterey, CA., July, 1996

12. G. Hickey, R. Manvi, and T. Knowles, "Phase change materials for advanced Mars thermal control," Proc. SAE 26th International Conference on Environmental Systems, Monterey, CA., July, 1996

13. P. S. Schenker, E. T. Baumgartner, S. Lee, H. Aghazarian, M. S. Garrett, R. A. Lindemann, D. K. Brown, Y. Bar-Cohen, S. S. Lih, B. Joffe, S. S. Kim, Jet Propulsion Lab.; B. H. Hoffman, Massachusetts Inst. Technology, "Dexterous robotic sampling for Mars in-situ science," in Intelligent Robots and Computer Vision XVI, SPIE Proc. 3208, Pittsburgh, PA, October, 1997; see also, P. S. Schenker, D. L. Blaney, D. K. Brown, Y. Bar-Cohen, S-S. Lih, R. A. Lindemann, E. D. Paljug, J. T. Slostad, G. K. Tharp, C. E. Tucker, C. J. Voorhees, and C. Weisbin, Jet Propulsion Lab.; E. T. Baumgartner, Mich. Tech. Univ.; R. B. Singer, R. Reid, Univ. of Arizona, "Mars lander robotics and machine vision capabilities for *in situ* planetary science," in Intelligent Robots and Computer Vision XIV, SPIE Proc. 2588, Philadelphia, PA, October, 1995; and, R. Volpe, T. Ohm, R. Petras, R. Welch, J. Balaram, R. Ivlev, "A prototype manipulation system for Mars rover science operations," Proc. IEEE/RSJ Intl. Conference on Intelligent Robots and Systems (IROS'97), Grenoble, France, September 7-11, 1997.

14. T. Ueha and Y. Tomikawa, *Ultrasonic Motors - Theory and Applications*, Oxford Science Publications, Oxford, England, 1993; also, J. Hollerbach, I. W. Hunter, and J. Ballantyne, "A comparative analysis of actuator technologies for robotics," in *Robotics Review 2 (eds. O. Khatib, J. Craig, and T. Lozano-Perez)*, The MIT Press, Cambridge, MA, 1992; JPL-specific developments are discussed in: Y. Bar-Cohen, S.-S. Lih and N. W. Hagood, "Solid-state actuation as a drive mechanism for miniature spacecraft," Proc. 9th Annual AIAA/USU Conf. on Small Satellites, Utah State University, Iowa, Sep 19-21, 1995; Y. Bar-Cohen, S.-S. Lih and N. W. Hagood, "Miniature ultrasonic rotary motors," Proc. AVS 2nd Micromachining Workshop, Anaheim, CA, September 19-21, 1995; S.-S. Lih and Y. Bar-Cohen "Rotary piezoelectric motors actuated by traveling waves," in Enabling Technologies: Smart Structures and Integrated Systems, SPIE Proc. 3041, San Diego, CA, March, 1997.

15. L. Matthies, T. Balch, and B. Wilcox, "Fast optical hazard detection for planetary rovers using multiple spot laser triangulation," Proc. 1997 Intl. IEEE Conf. on Robotics and Automation, Albuquerque, NM, April 20-25; L. Matthies et al., "Obstacle detection for unmanned ground vehicles: a progress report," Proc. 7th Intl. Symp. Robotics Research, Germany, October, 1996 (ref: Springer-Verlag, New York, NY, 1996, ISBN 3-540-76043-1); and, L. Matthies, C. Olson, G. Tharp, S. Laubach, "Visual localization methods for Mars rovers using lander, rover, and descent imagery," Intl. Symposium on Artificial Intelligence, Robotics, and Automation in Space (i-SAIRAS '97), Tokyo, Japan, July, 1997.